



## The optical parameters and memory switching of amorphous $\text{Se}_{70}\text{Te}_{15}\text{Bi}_{15}$ thin films

H.E. Atyia

Physics Department, Faculty of Education, Ain Shams University, Roxy, Cairo, (EGYPT)

E-mail : hebaelghrip@hotmail.com

### ABSTRACT

Films of  $\text{Se}_{70}\text{Te}_{15}\text{Bi}_{15}$  were deposited at room temperature, using thermal evaporation on the glass and pyrographite substrates. The X-ray diffraction pattern confirmed that  $\text{Se}_{70}\text{Te}_{15}\text{Bi}_{15}$  films have an amorphous nature. Optical properties of a- $\text{Se}_{70}\text{Te}_{15}\text{Bi}_{15}$  films were characterized by using spectrophotometric measurements of transmittance and reflectance in the spectral range (400-2500 nm). The refractive index dispersion curve shows an anomalous dispersion in the absorption region and a normal one in the transmitted region. Analysis of the dependence of absorption coefficient  $\alpha$  in the photon energy reveals allowed indirect transitions with energy gap  $\approx 1.72\text{eV}$ . Optical dispersion parameters according to Wemple and Didomenico model were determined. The temperature dependence of the electrical resistance shows parallel straight lines, which indicate single activation energy  $\Delta E_{\sigma}$  independent on the film thickness. Study of static and dynamic current voltage (I-V) characteristics for a- $\text{Se}_{70}\text{Te}_{15}\text{Bi}_{15}$  films reveals a memory switch. The mean value of switching voltage  $V_{th}$  increases with increasing the film thickness and decreases with increasing temperature. The value of switching voltage activation energy  $\varepsilon$  was calculated. The calculated ratio  $\varepsilon/\Delta E_{\sigma} = 0.54$  is nearly to be 0.5, obtained theoretically on the basis of electrothermal model. Therefore, the switching phenomenon in a- $\text{Se}_{70}\text{Te}_{15}\text{Bi}_{15}$  films can be explained according to a physical model based on the electrothermal breakdown theory. © 2014 Trade Science Inc. - INDIA

### KEYWORDS

Optical properties;  
a- $\text{Se}_{70}\text{Te}_{15}\text{Bi}_{15}$  films;  
Memory switching;  
Electrothermal model.

### INTRODUCTION

Amorphous chalcogenides have recently gained considerable attention due to their interesting optical and technological applications. These materials do not have long-range order, exhibit semiconductor's properties such as energy band gap, switching phenomenon and other electrical properties. These properties were discussed according to the presence of localized

states<sup>[1,2]</sup>. The knowledge of optical constants of materials is of great interest in the design and analysis of materials to be used in optoelectronics. Moreover, optical measurements are extensively used for characterization of composition and quality of the materials. The switching phenomenon is one of the numerous interesting effects arising in strong electric field<sup>[3]</sup>. Which is a rapid reversible transition between a highly resistive (OFF state) and a conductive (ON state). There are two types of

## Full Paper

electrical switching observed in amorphous chalcogenide, namely threshold and memory switching. In threshold switching, the ON state persists only while a current flows down to a certain holding voltage, whereas in memory switching, the ON state is permanent until a suitable reset current pulse is applied across the sample. Different mechanisms have been proposed to explain the switching phenomenon in chalcogenide glasses. These include electronic<sup>[4]</sup>, electrothermal<sup>[5]</sup> and thermal<sup>[6]</sup> mechanisms. In general threshold switching is electronic in origin, while memory switching is thermal origin<sup>[7]</sup>. The formation of highly conducting crystalline channels or filaments is considered as a possible cause of memory switching in the chalcogenide glasses<sup>[8]</sup>.

In this paper, the optical properties, electrical resistivity and switching phenomenon are reported and discussed for a- $\text{Se}_{70}\text{Te}_{15}\text{Bi}_{15}$  films.

### EXPERIMENTAL PROCEDURE

Bulk  $\text{Se}_{70}\text{Te}_{15}\text{Bi}_{15}$  chalcogenide glasses were prepared from high purity Se, Te and Bi elements weighted according to their stoichiometric ratio and sealed in an evacuated silica tube ( $10^{-5}$  Torr). The tube was heated in an oscillatory furnace. The temperature of the furnace was raised gradually to 1273 K with the rate 3–4 K  $\text{min}^{-1}$ , then this temperature kept constant for 15 h<sup>[9]</sup>. The tube is quenched in an icy water to obtain the samples in the glassy state. Thin films were obtained by thermal evaporation technique. Subsequent deposition on highly cleaned glass and pyrographite substrates for optical and switching measurements respectively. The thickness of films was measured during deposition using a thickness monitor (Edwards, FTM) and confirmed after deposition by Tolansky's interferometric method<sup>[10]</sup>.

The chemical composition of the studied films was checked by energy-dispersive X-ray analysis (EDX) by a scanning electron microscope (Joel 5400). Analysis of EDX spectrum showed that the composition of films are near  $\text{Se}_{70}\text{Te}_{15}\text{Bi}_{15}$ <sup>[9]</sup>.

X-ray diffraction pattern indicate that the investigated films have an amorphous nature. The amorphous structure of the deposited films on substrates kept at room temperature is expected. Because of that in the deposition process, the evaporated molecules precipi-

tate randomly on the surface of the substrate and all the following condensed molecules also adhere randomly leading to disordered films of increased thickness. The loss of adequate kinetic energy for the precipitated molecules keeps them unable to orient themselves to produce the chain structure, required for the crystalline structure. The internal stresses generated in the layers of the film due to the continuous deposition of the hot molecules on the cold pre-deposited layers increase both the disorder and the degree of randomness, which yields amorphous films whatever their thickness

The optical transmittance and reflectance of the films were measured at room temperature using a dual beam spectrophotometer (UV-3101 PC Shimadzu) in the wavelength range 400–2500 nm.

Thin film samples were sandwiched between two aluminum electrodes for dc electrical measurements. The electrical resistance  $R_{dc}$  was measured directly by a digital electrometer (Keithley model E616A). I–V characteristic curves were studied for a- $\text{Se}_{70}\text{Te}_{15}\text{Bi}_{15}$  films of different thicknesses at room temperature, as well as at elevated temperatures. For switching measurements, films were deposited on to pyrographite substrates, which is different from other shapes of graphite by its high density. Static I–V characteristics were measured in the usual way using a high impedance digital electrometer (Keithley 616) for potential drop measurements and a digital multimeter (TE924) for current measurements. Dynamic I–V characteristics were measured using an ac voltage source supplied from an autotransformer. The obtained I–V curve was seen on the screen of the cathode ray oscilloscope. For switching measurements a copper sample holder was used for point contact construction. The film sample was sandwiched between two electrodes of the cell. The upper electrode was movable and the lower one was made of a platinum needle having a circular brass disk end of diameter 0.2mm.

### RESULTS AND DISCUSSION

#### Optical properties of a- $\text{Se}_{70}\text{Te}_{15}\text{Bi}_{15}$ films

Transmittance T and reflectance R spectrum were measured at normal incidence in the wavelength range (400–2500 nm) for a- $\text{Se}_{70}\text{Te}_{15}\text{Bi}_{15}$  films in the thickness range (256–688 nm). The spectral distributions of

T and R were shown in Figure 1(a, b). One could note that at larger wavelength ( $\lambda > 1110$  nm) films become transparent where no light is absorbed ( $k = 0$ ) and the region at shorter wavelength ( $\lambda < 1110$  nm) i.e. ( $R+T < 1$ ) is known as absorbing region. To obtain the optical constants (refractive index  $n$  and absorption index  $k$ ) for the studied films, Murmann's<sup>[11]</sup> exact equations have been applied in conjunction with the special iterative computer program. This method requires approximate values of  $n$  and  $k$ . The approximate values of  $n_a$  and  $k_a$  were obtained using the Swanepoel method<sup>[12]</sup>. It is easy to solve Murmann's exact equations simultaneously using the experimental values of T and R to obtain the accurate values of  $n$  and  $k$ .

Values of refractive index  $n$  and absorption index  $k$  were computed for a- $\text{Se}_{70}\text{Te}_{15}\text{Bi}_{15}$  films with different thicknesses in the studied range. The variation of  $n$  and  $k$  with film thickness lie within the experimental error  $\pm 3\%$  for  $n$  and  $\pm 5\%$  for  $k$ . Accordingly both  $n$  and  $k$  are thickness independent. Figure 2 (a, b) show the spectral distribution of  $n$  and  $k$  for a- $\text{Se}_{70}\text{Te}_{15}\text{Bi}_{15}$  films in the wavelength range (400 - 2500 nm). It is clear that both  $n$  and  $k$  decrease with increasing  $\lambda$  except a peak was observed in  $n$  spectrum at  $\lambda = 600$  nm, indicating an anomalous dispersion in ( $\lambda < 660$  nm) as well as a normal dispersion in ( $\lambda > 660$  nm).

#### Determination of high frequency dielectric constant and dispersion energy parameters for a- $\text{Se}_{70}\text{Te}_{15}\text{Bi}_{15}$ films

The high frequency dielectric constant was obtained by analyzing the refractive index data via two proce-

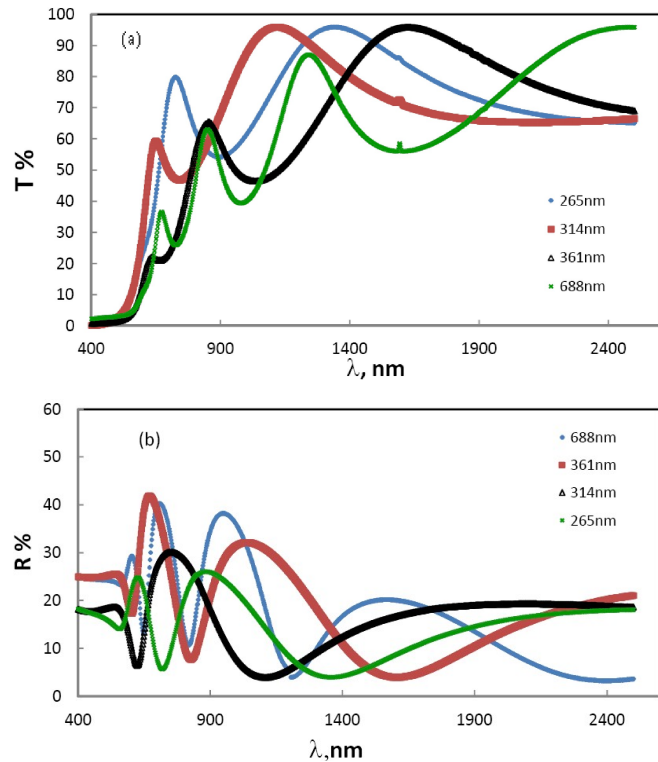


Figure 1 : Spectral behavior of the transmittance  $T(\lambda)$  (a) and the reflectance  $R(\lambda)$  (b) of a- $\text{Se}_{70}\text{Te}_{15}\text{Bi}_{15}$  films

dures<sup>[13]</sup>. In the first procedure the dielectric constant is partially due to the free carriers and the lattice vibration modes of the dispersion as represented by the following relation<sup>[14]</sup>.

$$\epsilon_1 = \epsilon_{\infty}(1) - \frac{e^2 N}{4\pi^2 C^2 \epsilon_0 m^*} \lambda^2 \quad (1)$$

where  $\epsilon_1$  is the real part of dielectric constant,  $\epsilon_{\infty}(1)$  is the lattice dielectric constant or (the high frequency

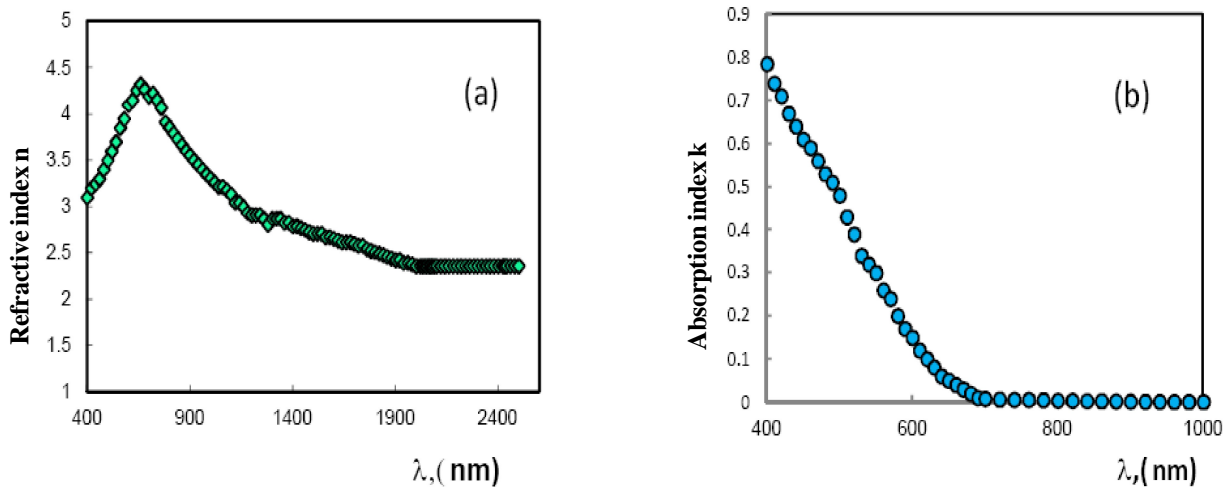


Figure 2 : Spectral dependence of refractive index  $n$  (a) and absorption index  $k$  (b) of a- $\text{Se}_{70}\text{Te}_{15}\text{Bi}_{15}$  films

## Full Paper

dielectric constant) according to first procedure,  $N$  is the free charge carrier concentration,  $\epsilon_0$  is the permittivity of free space ( $8.854 \times 10^{-12}$  F/m),  $m^*$  is the effective mass of the charge carrier and  $c$  is the velocity of light. Figure 3 represented the plotted of  $n^2(\epsilon_1 = n^2)$  as a function of  $\lambda^2$  for a- $\text{Se}_{70}\text{Te}_{15}\text{Bi}_{15}$  films. A linear relation was obtained at longer wavelength. Both values of  $\epsilon_\infty(1)$  and  $N/m^*$  were calculated from Figure 3 and given in TABLE 1. The second procedure is based upon the dispersion arising from the bound carriers in an empty lattice,  $\epsilon_\infty(2)$  can be calculated using the following equation<sup>[13]</sup>

$$\frac{n_0^2 - 1}{n^2 - 1} = 1 - \frac{\lambda_0^2}{\lambda^2} \quad (2)$$

where  $n_0$  is the refractive index at infinite wavelength

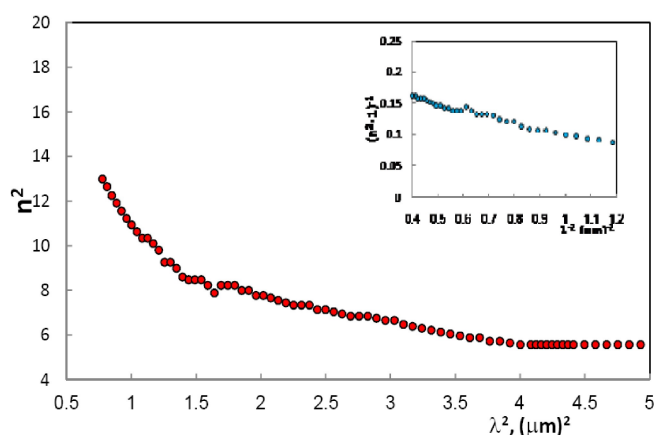


**Figure 3 :** Plots of  $n^2$  vs.  $\lambda^2$  for a- $\text{Se}_{70}\text{Te}_{15}\text{Bi}_{15}$  films. the inset figure represents the plot of  $(n^2 - 1)^{-1}$  against  $\lambda^{-2}$  for a- $\text{Se}_{70}\text{Te}_{15}\text{Bi}_{15}$  films.

**TABLE 1 :** Parameters obtained from the analysis of refractive index  $n$  data for a- $\text{Se}_{70}\text{Te}_{15}\text{Bi}_{15}$  films.

Parameter	Value
$\epsilon_\infty(1)$	7.9
$\epsilon_\infty(2)$	7.5
$\lambda_0$ , (nm)	316
$S_o$ , ( $\text{m}^{-2}$ )	$6.57 \times 10^{13}$
$E_o$ , (eV)	2.02
$E_{d_1}$ , (eV)	11.38
$E_o/S_o$ , ( $\text{eV m}^2$ )	$3.12 \times 10^{-14}$
$N/m^*$ , ( $\text{kg}^{-1}\text{m}^{-3}$ )	$10.2 \times 10^{56}$
$f$ , ( $\text{eV}^2$ )	23.33

and  $\lambda_0$  average inter-band oscillator wavelength. Plotting of  $(n^2 - 1)^{-1}$  against  $\lambda^{-2}$  as shown in the inset Figure 3, values of  $\epsilon_\infty(2)$  and  $\lambda_0$  can be calculated and tabulated in TABLE 1. From the above results the obtained values  $\epsilon_\infty(1)$  and  $\epsilon_\infty(2)$  agree with each other, which may be due to that the lattice vibrations and bounded carriers in an empty lattice are in the transparent region<sup>[15,16]</sup>. Equation (2) can also be written as<sup>[17]</sup>:

$$(n^2 - 1) = \left( \frac{S_o \lambda_0^2}{1 - \lambda^2 / \lambda_0^2} \right) \quad (3)$$

Where  $S_o = (n_0^2 - 1) / \lambda_0^2$  is the average oscillator strength. Value of  $S_o$  is illustrated in TABLE 1.

The energy dependence of refractive index  $n$  for a- $\text{Se}_{70}\text{Te}_{15}\text{Bi}_{15}$  films can be fitted by using the single oscillator model in the normal dispersion region developed by Wemple and Didomenico (WDD) model<sup>[18,19]</sup>

$$n^2 = 1 + \frac{E_o E_d}{E_0^2 - (hv)^2} \quad (4)$$

Where  $E_o$  the single-oscillator energy and  $E_d$  the so-called dispersion energy. Both energies were obtained by plotting  $(n^2 - 1)^{-1}$  vs.  $(hv)^2$  for a- $\text{Se}_{70}\text{Te}_{15}\text{Bi}_{15}$  films as shown in Figure 4. Values of  $E_o$ ,  $E_d$  and  $E_o/S_o$  were calculated and given in TABLE 1. This value of  $E_o/S_o$  is approximately in the same order as obtained by WDD model<sup>[18,19]</sup> ( $E_o/S_o = 6.0 \pm 0.5 \times 10^{-14}$  eV.m<sup>2</sup>) for a number of materials. There is an important parameter called the oscillator strength ( $f$ ) is reported in<sup>[20,21]</sup> such that  $f = E_o E_d / (eV)^2$ . For studied films, value of ( $f$ ) was given in TABLE 1.

The optical properties of a- $\text{Se}_{70}\text{Te}_{15}\text{Bi}_{15}$  films could be described through the dielectric function  $\epsilon^* = \epsilon_r + i\epsilon_i$ ,

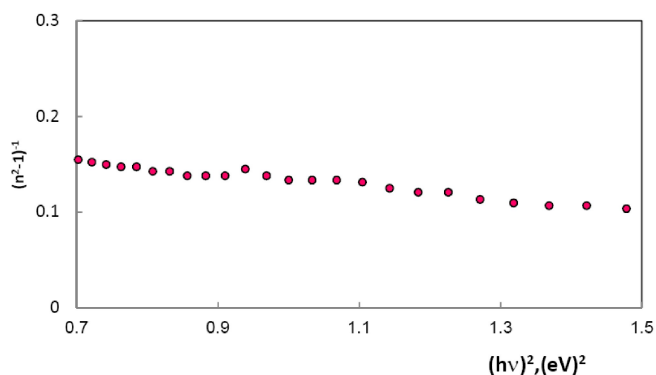


**Figure 4 :** Plots of  $(n^2 - 1)^{-1}$  vs.  $(hv)^2$  for a- $\text{Se}_{70}\text{Te}_{15}\text{Bi}_{15}$  films

where  $\epsilon_r$  and  $\epsilon_i$  are real and imaginary parts of complex dielectric constant respectively.  $\epsilon_r$  and  $\epsilon_i$  were determined by the following relation<sup>[22]</sup>  $\epsilon_r = n^2 - k^2$  and  $\epsilon_i = 2nk$ . Variation of  $\epsilon_r$  and  $\epsilon_i$  with photon energy was represented in Figure 5. It is clear that values of  $\epsilon_r$  are higher than that of  $\epsilon_i$  and both of them have a same behavior at low photon energy, except a peak was appeared in  $\epsilon_r$  spectrum at photon energy = 1.88 eV.

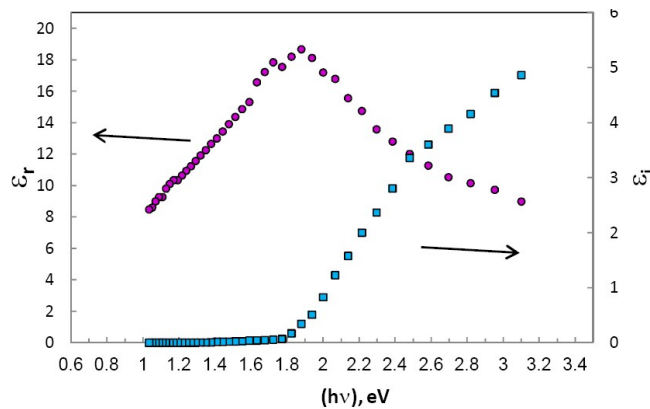


Figure 5 : Plot of  $\epsilon_r$  and  $\epsilon_i$  vs.  $(h\nu)$  for a- $\text{Se}_{70}\text{Te}_{15}\text{Bi}_{15}$  films.

### Energy gap determination

The absorption coefficient  $\alpha$  was calculated from the well-known equation,  $\alpha = 4\pi k/\lambda$  for a- $\text{Se}_{70}\text{Te}_{15}\text{Bi}_{15}$  films. Hence the spectral of  $\alpha$  can be divided in to two region. The first region for lower values of  $\alpha < 10^4 \text{ cm}^{-1}$ , where the absorption usually follows the Urbach's rule<sup>[23]</sup> according to the following equation:

$$\alpha(\nu) = \alpha_0 \exp \frac{h\nu}{E_e} \quad (5)$$

Where  $\alpha_0$  is a constant and  $E_e$  is the Urbach's energy which is interpreted as the width of the tails of localized

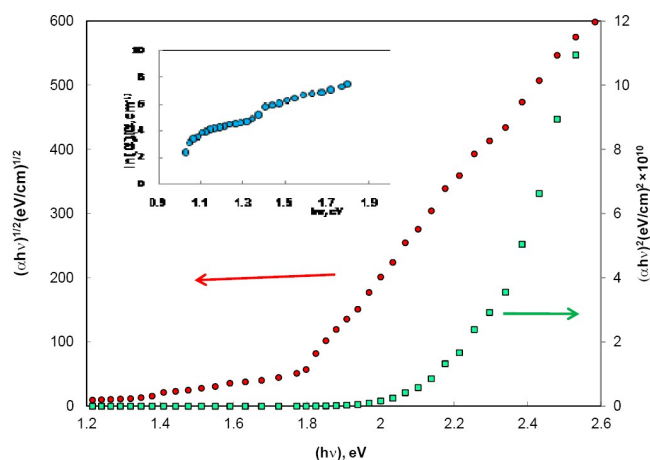


Figure 6 : Dependence of  $(\alpha h\nu)^{1/2}$  and  $(\alpha h\nu)^2$  of photon energy  $(h\nu)$  for a- $\text{Se}_{70}\text{Te}_{15}\text{Bi}_{15}$  films, the inset figure represents the plot of  $\ln(\alpha)$  vs.  $(h\nu)$  for a- $\text{Se}_{70}\text{Te}_{15}\text{Bi}_{15}$  films.

states in the band gap. To determine the values of  $\alpha_0$  and  $E_e$ ,  $\ln \alpha$  was plotted as a function of  $h\nu$  as shown in the inset Figure 6. The second region for  $\alpha > 10^4 \text{ cm}^{-1}$ , the optical absorption edge was analyzed by the following relation<sup>[24]</sup>:

$$\alpha h\nu = A(h\nu - E_{g(1)}^{opt})^r \quad (6)$$

where  $A$  is a constant,  $E_{g(1)}^{opt}$  is the optical energy gap and  $r$  is the power which characterizes the transition process, has the value 1/2 or 2 for direct or indirect allowed transitions respectively. To determine the value of  $E_{g(1)}^{opt}$  and the type of transitions,  $(\alpha h\nu)^{1/2}$  and  $(\alpha h\nu)^2$  were plotted versus  $h\nu$  as shown in Figure 6. The linearity of  $(\alpha h\nu)^{1/2} = f(h\nu)$  indicating the existence of indirect allowed transitions. Values of  $\alpha_0$ ,  $E_e$ ,  $A$  and  $E_{g(1)}^{opt}$  were given in TABLE 2.

The obtained value of  $E_{g(1)}^{opt}$  can be confirmed by plotting  $h\nu \sqrt{\epsilon_i}$  vs.  $h\nu$  near the absorption edge as shown in Figure 7, according to the relation<sup>[25]</sup>

$$h^2\nu^2\epsilon_i \approx (h\nu - E_{g(2)}^{opt})^2 \quad (7)$$

The obtained linearity indicates indirect optical transitions<sup>[25]</sup>. The extrapolations of this linear part yield  $E_{g(2)}^{opt}$  for a- $\text{Se}_{70}\text{Te}_{15}\text{Bi}_{15}$  films. The obtained value of

TABLE 2 : Parameters obtained from the analysis of absorption index  $k$  data for a- $\text{Se}_{70}\text{Te}_{15}\text{Bi}_{15}$  films.

Parameter	Value
$\alpha_0, \text{cm}^{-1}$	0.049
$E_e, (\text{eV})$	0.221
$A, \text{cm}^{-1} \text{eV}^{-1}$	$4.4 \times 10^5$
$E_{g(1)}^{opt} (\text{eV})$	1.73
$E_{g(2)}^{opt} (\text{eV})$	1.71

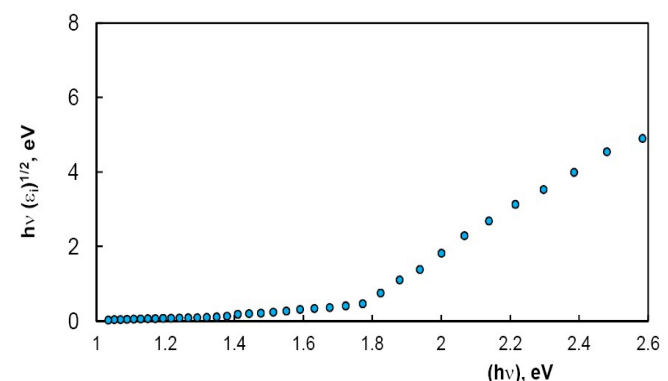


Figure 7 : Dependence of  $h\nu(\epsilon_i)^{1/2}$  on the photon energy  $(h\nu)$  for a- $\text{Se}_{70}\text{Te}_{15}\text{Bi}_{15}$  films.

## Full Paper

$E_{g(2)}^{opt}$  from Figure 7 was given in TABLE 2, which is in good agreement with that obtained by plotting  $(\alpha hv)^{1/2}$  vs.  $hv$  for indirect allowed transitions. The obtained average value of  $E_{g(2)}^{opt}$  (1.72 eV) for studied a- $Se_{70}Te_{15}Bi_{15}$  films can be compared with that obtained before for  $Se_{85}Te_{15}$  (1.09 eV)<sup>[26]</sup> and for  $Se_{85}Te_{10}Bi_5$  (1.32 eV)<sup>[27]</sup>. It is clear that the addition of Bi As a third element of  $Se_{85}Te_{15}$  films increases the energy gap and the increase of Bi % leads to further increasing in energy gap. The observed change of energy gap can be understood according to modify the structure, electrical and optical properties of Se-Te glasses with the addition of Bi as third element. In particular, introduction of Bi leads to enhance the disorder in the system and hence leads to deeper penetration of the localized states into energy gap<sup>[28,29]</sup>. In the same time there is an increase in the density of bonds between Se (the host element) and the addition of Bi metal stronger than other Se-Se bonds<sup>[30]</sup>

### Electrical resistivity for a- $Se_{70}Te_{15}Bi_{15}$ films

The temperature dependence of a- $Se_{70}Te_{15}Bi_{15}$  film resistance was studied in the temperature range 303–393 K below  $T_g$  and thickness range 219 – 445 nm. Figure 8 shows the plot of film resistance R vs. temperature. It can be seen that the resistance decreases as the temperature increases showing normal chalcogenide behavior of exponential decrease of R with temperatures. The temperature dependence of the dc electrical conductivity  $\sigma_{dc} = \frac{1}{R} \frac{t}{a}$  (where a the cross-section area and t the film thickness) was given by the following relation

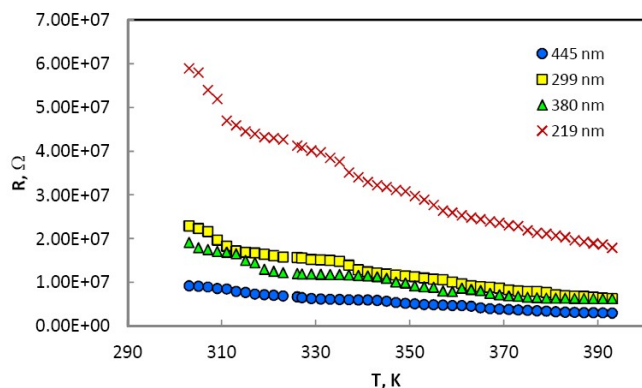


Figure 8 : Variation of the film resistance R vs. T for a- $Se_{70}Te_{15}Bi_{15}$  films at different thicknesses.

$$\sigma = \sigma_0 \exp\left(\frac{-\Delta E_\sigma}{k_B T}\right) \quad (8)$$

which can be rewritten as

$$R = R_0 \exp\left(\frac{\Delta E_\sigma}{k_B T}\right) \quad (9)$$

where  $\sigma_0$  is the pre-exponential factor,  $k_B$  the Boltzmann constant and  $\Delta E_\sigma$  the conduction activation energy.  $\Delta E_\sigma$  was determined by plotting  $\ln(R)$  against  $1000/T$  as shown in Figure 9. The obtained parallel straight lines indicate that the conduction in a- $Se_{70}Te_{15}Bi_{15}$  film is thermally activated process with single activation energy  $\Delta E_\sigma = 0.192 \pm 0.004$  eV independent of film thickness in the studied range. The obtained value of  $\Delta E_\sigma$  is in a good agreement with that obtained before<sup>[9]</sup> from AC measurements. It is clear also that the resistance R decreases with increasing film thickness this may be due to the decrease of the density of lattice defects developed through film deposition, thus the resistivity is decrease with increasing film thickness<sup>[31]</sup>.

### Switching properties of a- $Se_{70}Te_{15}Bi_{15}$ films

#### Dynamic and static I-V characteristics

Both dynamic and static I-V characteristic curves for a- $Se_{70}Te_{15}Bi_{15}$  films deposited on cleaned and highly polished pyrographite substrates were shown in Figure 10 (a,b) of film thicknesses 299 and 445 nm respectively as an example. It is observed that by increasing the applied voltage a very small current is obtained forming the first branch (oa) of the I-V curve, The branch (oa) represents the OFF state (with high resistance state) of the switch, which can be divided into 3 subregions o-f, f-g, g-a as shown in inset Figure 10 (b). The first region is linear (ohmic conduction), the second is exponential fol-

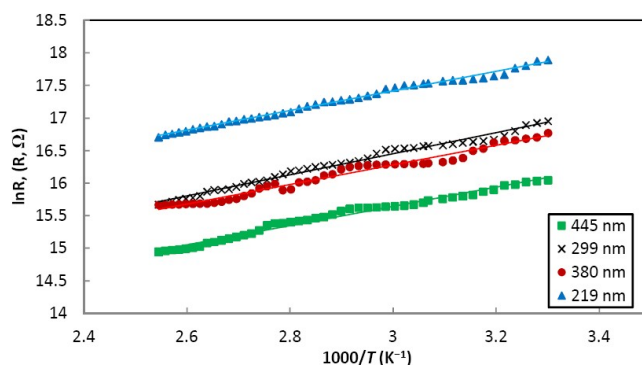
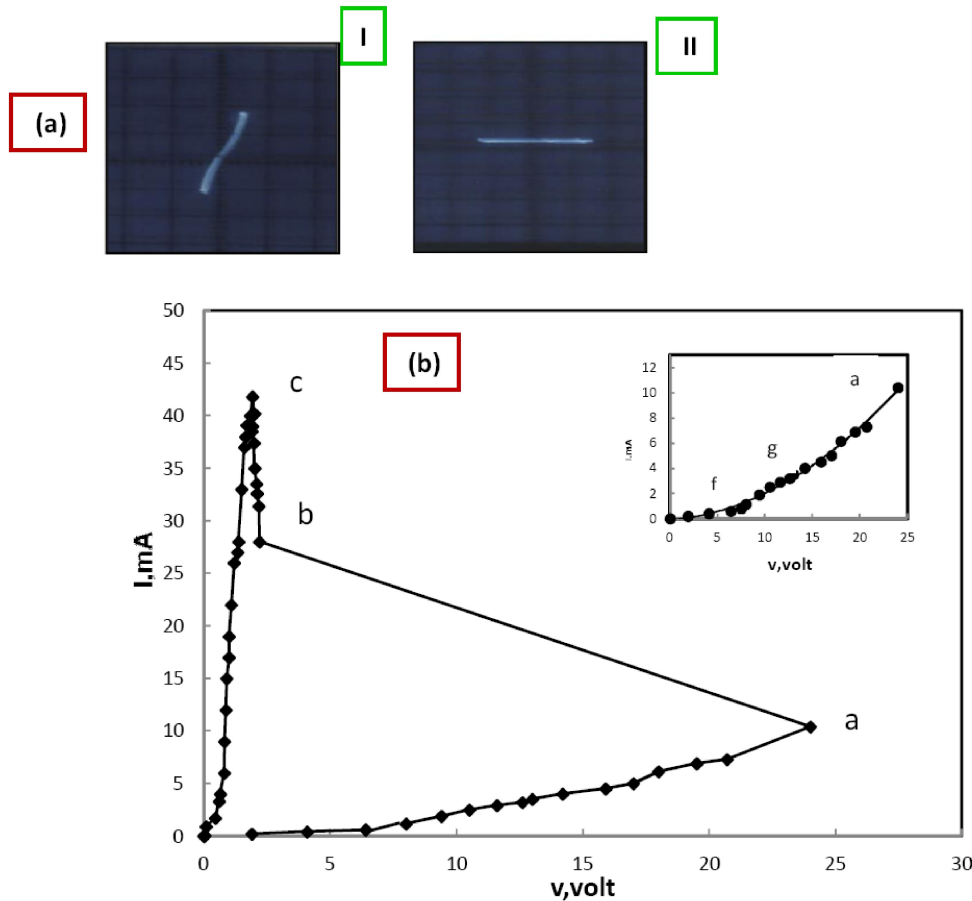


Figure 9 : Plots of  $\ln(R)$  against  $1000/T$  for a- $Se_{70}Te_{15}Bi_{15}$  films with different thicknesses.



**Figure 10 :** (a) Dynamic I–V characteristics of a- $\text{Se}_{70}\text{Te}_{15}\text{Bi}_{15}$  films of thickness 299 nm (I) ON-state; (II) OFF-state. (b) Static I–V characteristics of a- $\text{Se}_{70}\text{Te}_{15}\text{Bi}_{15}$  film of thickness 445nm, the inset figure represent the OFF- state of the static I-V characteristic curve of film thickness 445 nm.

lowing the Pool-Frenkel relation  $\{I=I_0 \exp (V/V_0)^{1/2}\}$  and the third verifying the formula  $\{I=I_0 \exp (V/V_0)\}$ <sup>[32]</sup>

At the point(a) a sudden increase in the current and drop in voltage to the point (b), i.e. switching occurs, through the load line ab (negative resistance region). This critical value of the applied voltage is called the switching voltage  $V_{th}$ . Switching process takes place in a very short time ( $\approx 10^{-9}$  s). So it is impossible to record any reading during this time (the part ab of the curve). A more increase in the applied voltage increases the current without any significant increase in the potential drop (part bc). This (bc) part of the curve is called the ON state (with low resistance) or the holding branch. At point c, further decrease in the applied voltage cause a decrease in the current until finally both become zero (part co of the curve). The obtained curve is a typical I–V characteristic for a memory switch, similar to that of many chalcogenide glasses<sup>[27,31,33]</sup>. In memory devices the investigated films sustain their high conduction state (ON state) after switch-

ing. The structural change accrues in microcrystalline state after switch ON. This crystallization processes may be caused by Joule- heating due to high filed and excess carrier concentration. A memory switching exhibited in a- $\text{Se}_{70}\text{Te}_{15}\text{Bi}_{15}$  films was in contrast to threshold switching glass compositions which have a stable structure and does not exhibit a reversible change between amorphous and crystalline phases

### Thickness dependence of the mean value of switching voltage $V_{th}$

Room temperature I–V curves of a- $\text{Se}_{70}\text{Te}_{15}\text{Bi}_{15}$  films were studied of different thicknesses in the range (219 – 445 nm). The obtained results were shown in Figure 11. It is observed that  $V_{th}$  increases with increasing film thickness. The thickness dependence of  $V_{th}$  can be explained by the increasing of film conductance or decrease of film resistance. The dependence of the mean value of the switching voltage  $V_{th}$  measured at different temperature on the film thickness was illustrated in the

## Full Paper

inset Figure 11. It is clear from this figure that  $V_{th}$  increasing linearly with film thickness with the mean value of the threshold field  $E_{th} = 4.5 \times 10^7$  V/m.

### Temperature dependence of the mean value of switching voltage $V_{th}$

The obtained I–V curves were illustrated in Figure 12 for a- $Se_{70}Te_{15}Bi_{15}$  film of thickness 445 nm as a representative example at different temperature in the range (303 – 393 K). It is clear that the obtained I–V curves at elevated temperatures are also typical for the memory switching phenomenon. Values of  $V_{th}$  decrease exponentially with increasing temperature as shown in inset Figure 12. This may be due to that, if the temperature increases, the thermal energy required for the transformation of the channel material (filament) from the

amorphous to crystalline state will be lower. Therefore, the magnitude of the switching voltage  $V_{th}$  decreases with the increase of the temperature.

Most of amorphous materials contain dipoles dispersed randomly throughout the amorphous matrix. As the electric field is applied, these dipoles tend to orient in the direction of the field. The orientation process depends on the viscosity of the amorphous matrix as well as the applied field<sup>[34]</sup>. As the temperature of the conduction path increases its viscosity decreases, which leads to an increase in the orientation processes up to switching point. At this point, the resultant force of resistance for dipole orientation in viscous amorphous medium diminishes. Thus, switching process takes place.

A plot of  $\ln V_{th}$  versus  $1000/T$  for a- $Se_{70}Te_{15}Bi_{15}$  with different thicknesses was illustrated in Figure 13. The obtained relation yield straight lines satisfying the following relation<sup>[35]</sup>:

$$V_{th} = V_0 \exp\left(\frac{\epsilon}{k_B T}\right) \quad (10)$$

where  $V_0$  is constant and  $\epsilon$  is the switching voltage activation energy. The obtained straight lines in Figure 13 are parallel indicating that the switching voltage activation energy has a single value independent of film thickness. The calculated values of  $\epsilon$  and  $\epsilon/\Delta E_{\sigma}$  were given in TABLE 3. It is found that the ratio  $\epsilon/\Delta E_{\sigma} \approx 0.5$  agrees with that obtained theoretically on the basis of the electrothermal model for the switching process<sup>[35]</sup> and those obtained before for other semiconducting compositions<sup>[27,31,33, 37,38]</sup>. Then we can conclude that the observed memory switching type can be interpreted on

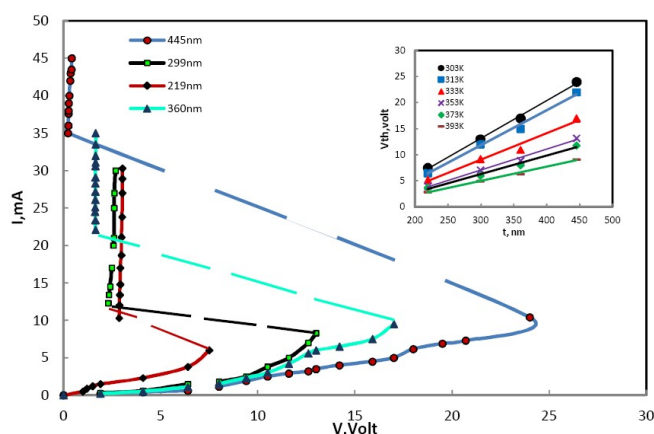


Figure 11 : Room temperature I–V characteristic curves of a- $Se_{70}Te_{15}Bi_{15}$  films of different thicknesses. The inset figure shows the thickness dependence of mean value of threshold voltage  $V_{th}$  of a- $Se_{70}Te_{15}Bi_{15}$  films at different temperatures.

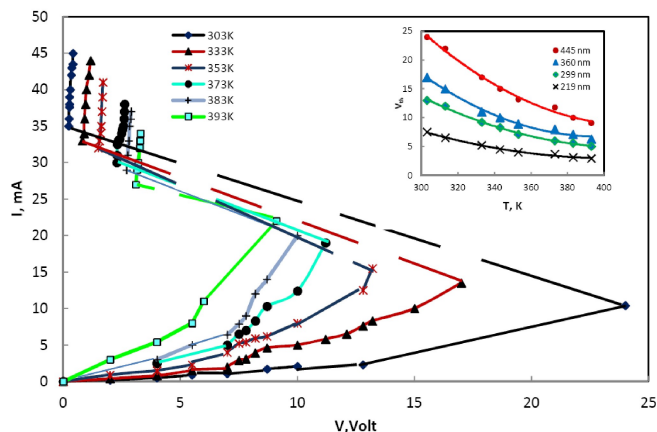


Figure 12 : Static I–V characteristic curves of a- $Se_{70}Te_{15}Bi_{15}$  films of thickness (445 nm) at different temperatures, the inset figure represents the temperature dependence of mean value of  $V_{th}$  of a- $Se_{70}Te_{15}Bi_{15}$  film at different thicknesses.

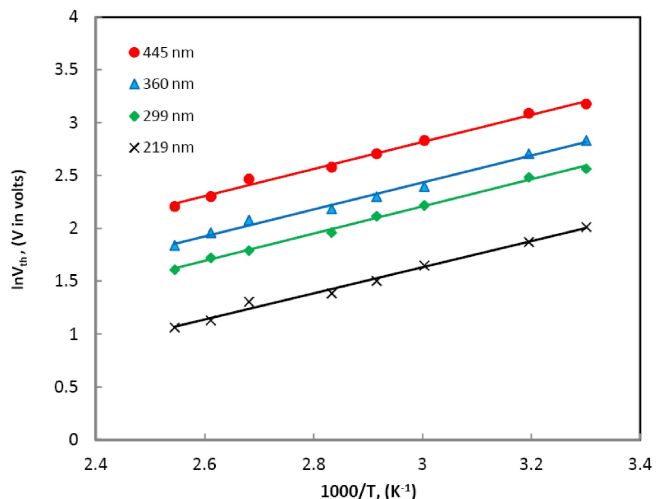


Figure 13 : Plots of  $\ln V_{th}$  vs.  $1000/T$  for a- $Se_{70}Te_{15}Bi_{15}$  films of different thicknesses

the basis of electrothermal breakdown process<sup>[39]</sup>. Values of the switching resistance  $R_{th}$  were obtained from the values of  $V_{th}$  and  $I_{th}$ . The temperature dependence of  $R_{th}$  for a- $Se_{70}Te_{15}Bi_{15}$  films yield straight lines as shown in Figure 14 obeying the following equation<sup>[40]</sup>:

$$R_{th} = R_0 \exp\left(\frac{\Delta E_R}{k_B T}\right) \quad (11)$$

where  $R_0$  is a constant and  $\Delta E_R$  is the switching resistance activation energy. The value of  $\Delta E_R$  was deduced using least-square fitting and given in TABLE 3. It is clear that  $\Delta E_R$  have a value in the same order with that of  $\Delta E_\sigma$  and  $\epsilon$ .

The switching process can be understood in terms

**TABLE 3 : Values of the switching parameters for a- $Se_{70}Te_{15}Bi_{15}$  films.**

Parameter	value
$\epsilon$ , (eV)	0.105±.009 eV
$(\epsilon / \Delta E_\sigma)$	0.54
$\Delta E_R$ , (eV)	0.204±.01 eV

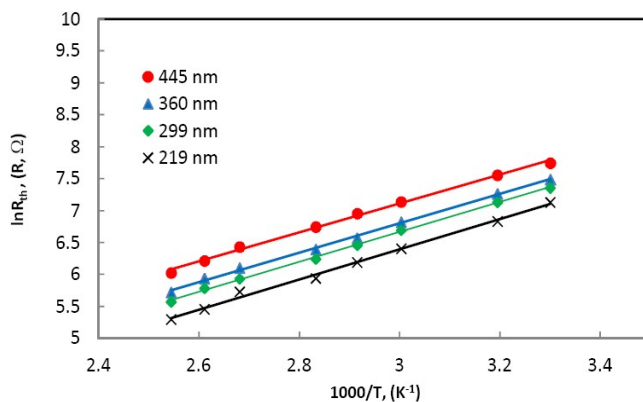


**Figure 14 : Plot of  $\ln R_{th}$  vs.  $1000/T$  for a- $Se_{70}Te_{15}Bi_{15}$  films of different thicknesses**

**TABLE 4 : Values of  $\Delta T_{breakdown}$  and  $T_m$  for a- $Se_{70}Te_{15}Bi_{15}$  films.**

$\Delta T_{breakdown}$ , (K)	$T_m$ , (K)
55.4	358.4
59.1	372.1
62.9	385.9
66.9	399.9
71.0	414.0
75.2	428.2
79.5	442.5
83.9	456.9
88.5	471.5
93.2	486.2

of electrothermal process based on Joule heating effect. Since the conduction process in amorphous semiconductor materials is of the thermally activated type, the sample conductivity  $\sigma$  was increased on heating. This allows the flow of higher current through the heated region as well as more Joule heating resulting in a further increase in the current density. Ultimately the temperature rise will become adequate to initiate a thermal breakdown owing to the strong temperature dependence of  $\sigma$ . A stationary state was reached when the heat lost by the conduction from the current filament becomes equal to the Joule heat generated in the heated region. The electrothermal model can be solved to a certain extent by finding a stationary state solution for the heat transport equation is

$$C \left(\frac{dT}{dt}\right) = \sigma E_{th}^2 + \nabla \cdot (\Psi \Delta T) \quad (12)$$

where  $C$  is the heat capacity of the sample,  $\Psi$  is the thermal conductivity coefficient of the samples and  $\sigma$  is the electrical conductivity given by equation 8. The charge conservation equation is<sup>[41]</sup>:

$$-\frac{1}{\sigma} \frac{d\rho}{dt} = \nabla \cdot E \quad (13)$$

where  $\rho$  is the charge density.

In the case of steady state breakdown, the time derivative of temperature  $\frac{dT}{dt}$  can be neglected in the solution of equation 12. Therefore equation 12 can be rewritten as follows<sup>[35]</sup>

$$8\Psi(\Delta T/d^2) + \sigma_{dc} E_{th}^2 = 0 \quad (14)$$

Then, the heat conduction equation for a small difference between the temperature of the middle of the specimen  $T_m$  and that of the surface  $T_s$

$$\Delta T_{breakdown} = T_m - T_s \quad (15)$$

The steady state breakdown occurs when the amount of heat generated by Joule heating in the specimen cannot be removed by thermal conduction. The temperature difference for breakdown obtained with the help of equations 8 and 14 is given by

$$\Delta T_{breakdown} = T_s^2 k_B / \Delta E_\sigma \quad (16)$$

Values of  $\Delta T_{breakdown}$  were calculated for film samples at different temperatures. Finally, from the above results. It can be concluded that the studied memory switching in a- $Se_{70}Te_{15}Bi_{15}$  films can be ex-

## Full Paper

plained according to the electrothermal model.

### CONCLUSIONS

Films of amorphous  $Se_{70}Te_{15}Bi_{15}$  were grown by thermal evaporation technique. The optical constants  $n$  and  $k$  of a- $Se_{70}Te_{15}Bi_{15}$  films were found to be independent of thickness in the range (256–688 nm). The values of the optical band gap  $E_g^{opt}$  and Urbach's energy  $E_c$  were calculated using the optical method. The type of optical transition responsible for optical absorption is allowed indirect transitions. The oscillator strength, oscillator energy and static dielectric constant were calculated by the analyzes of the refractive index data using Wemple and Didomenico model. Values of real part of the dielectric constant  $\epsilon_r$  were found higher than imaginary part  $\epsilon_i$ . The temperature dependence of the film resistance indicated that the electrical conduction activation energy  $\Delta E_c$  has a single value for all thicknesses indicating the presence of one conduction mechanism through the studied range of temperature. Dynamic and static (I-V) characteristics of a- $Se_{70}Te_{15}Bi_{15}$  films showed a typical memory switching phenomenon. The mean value of the switching voltage increases linearly with increasing film thickness and decreases exponentially with increasing temperature. The data obtained for switching characteristics were satisfactorily interpreted by the electrothermal model of the breakdown process.

### REFERENCES

- [1] R.A.Street, N.F.Mott; Phys.Rev.Lett., **35**, 1293 (1975).
- [2] M.Kastner, H.Fritzsche; Phil.Mag., **37**, 553 (1978).
- [3] R.Lokesh, N.K.Udayashankar, S.Asokan; J.Non-Cryst.Solids, **356**, 321 (2010).
- [4] D.Adler, M.S.Shur, M.Silver, S.R.Ovshinsky; J.Appl.Phys., **51**, 3289 (1980).
- [5] D.Adler; Sci.Am., **36**, 236 (1977).
- [6] H.Fritzsche, S.R.Ovshinsky; J.Non-Cryst.Solids, **4**, 464 (1970).
- [7] R.Rajesh, J.Philip; Semicond.Sci.Technol., **18**, 133 (2003).
- [8] A.S.Soltan, A.H.Moharram; J.Phys.: Condens. Matter, **349**, 92 (2004).
- [9] H.E.Atyia; Acta Physica Polonica, **125**, (2014).
- [10] S.Tolansky; Introduction to Interferometry, Longman, London, (1955).
- [11] M.Murmann; Z.Phys., **80**, 161 (1933); Ibid, **101**, 643 (1936).
- [12] R.Swanepoel; J.Phys.E.Sci.Instrum., **16**, 1214 (1983).
- [13] J.N.Zemel, J.D.Jensen, R.B.Schoolar; Phys.Rev.A, **140**, 330 (1965).
- [14] G.A.Kumar, J.Thomas, N.George, B.A.Kumar, P.Radhrishnan, V.P.N.Nampoori, G.P.G.Vallabham; Phys.Chem.Glasses, **41**, 89 (2000).
- [15] H.E.Atyia; J.Optoelectron.Adv.Mater, **8**, 1359 (2006).
- [16] M.M.Abdel-Aziz, I.S.Yahia, L.A.Wahab, M.Fadel, M.A.Afifi; Appl.Surf.Sci., **8**, 8163 (2006).
- [17] P.A.Lee, G.Said, R.Davis, L.T.Lim; J.Phys.Chem. Solids, **30**, 2719 (1969).
- [18] S.H.Wemple, M.Didomenico; Phys.Rev., **B7**, 3767 (1973).
- [19] S.H.Wemple, M.Didomenico; Phys.Rev., **B3**, 1338 (1971).
- [20] S.H.Wemple, M.Didomenico; Jr.Phys.Rev.Lett., (1969).
- [21] M.M.El-Nahass, M.M.Sallam, S.A.Rahman, E.M.Ibrahim; Solid State Science, **8**, 488 (2006).
- [22] M.M.Wakkad, E.Kh.Shokr, S.H.Mohamed; J.Non-Crystal.Solids, **265**, 157 (2000).
- [23] F.Urbach; Phys.Rev., **92**, 324 (1953).
- [24] J.Tauc; Amorphous and Liquide Semi-conducteurs, Plenum press, New York, 159 (1974).
- [25] J.Tauc, R.Grigorovici, A.Vancu; Phys.Stat.Sol., **15**, 627 (1966).
- [26] E.Marquez, T.Wagner, J.M.Gonza, A.M.Bernal-Olire, R.Prieto-Aleon, R.Jimenez-Garay, P.J.S.Ewen; J.Non-Crystal.Solides, **8**, 831 (1972).
- [27] H.E.Atyia, A.E.Bekheet; Physica, **B403**, 3130 (2008).
- [28] N.F.Mott; Philos.Mag., **34**, 1101 (1976).
- [29] N.F.Mott; Philos.Mag., **36**, 413 (1977).
- [30] L.Pauling; The Chemical Bond, Cornell University Press, Ithaca, NY, (1960).
- [31] M.A.Afifi, N.A.Hegab, H.E.Atyia, A.S.Farid; J.Alloys Compd., **463**, 10 (2008).
- [32] M.A.Afifi, H.H.Labib, N.A.Hegab, M.Fadel, A.E.Bekheet; Indian J.of Pure & applied Physics, **33**, 129 (1995).
- [33] H.E.Atyia; Physica, **B403**, 16 (2008).
- [34] S.Abou El-Hassan, H.Khader; Phys.Status Solidi (a), **186**, 401 (2001).
- [35] R.Mehra, R.Shyam, P.C.Mathur; J.Non-Cryst.Solids, **31**, 435 (1979).

- [36] K.W.Boer, S.R.Ovshinsky; J.Appl.Phys., **41**, 6 (1970).  
[37] A.E.Bekheet; Eur.Phys.J.-Appl.Phys., **16**, 187 (2001).  
[38] M.A.Afifi, N.A.Hegab, H.E.Atyia, M.I.Ismael; Vacuum, **83**, 326 (2009).  
[39] M.A.Afifi, N.A.Hegab; Vacuum, **48**, 135 (1997).  
[40] N.F.Mott; Phil.Mag., **22**, 7 (1970).  
[41] K.Shimakawa, Y.Inagaki, T.Arizumi; Jpn.J.Appl. Phys., **12**, 1043 (1973).